

Deep learning for classifying dynamical states from time series via recurrence plots

Athul Mohan^{1,2}, G. Ambika², Chandrakala Meena^{1,2}

¹ *Indian Institute of Science Education and Research (IISER), Pune, India and*

² *Indian Institute of Science Education and Research (IISER), Thiruvananthapuram, India*

(Dated: June 24, 2025)

Recurrence Quantification Analysis (RQA) is a widely used method for capturing the dynamical structure embedded in time series data, relying on the analysis of recurrence patterns in the reconstructed phase space via recurrence plots. Although RQA proves effective across a range of applications, it typically requires the computation of multiple quantitative measures, making it both computationally intensive and sensitive to parameter choices. In this study, we adopt an alternative approach that bypasses manual feature selection and extraction by directly using recurrence plot images as input to a deep learning model. We propose a new dual-branch deep learning architecture specifically designed to efficiently capture the complex dynamical features encoded in RPs. We also compare its performance against a baseline ResNet-50 model for classifying the dynamical behavior of time series using recurrence plots. Our dual-branch model, trained exclusively on simulated time series, accurately and efficiently distinguishes among six distinct classes: periodic, quasi-periodic, chaotic, hyperchaotic, white noise, and red noise. To assess its generalizability, we apply the trained model to time series generated from standard Lorenz and Rössler systems, neither of which is included in the training set, as well as to experimental datasets from a Chua circuit and observational light curves of the variable stars AC Her, SX Her, and Chi Cygni. In all cases, the model outperforms the baseline and yields predictions that align with the known dynamics of these systems. These results further demonstrate the robustness and versatility of our deep learning framework, underscoring the potential of RP based models as fast, accurate, and scalable tools for classifying dynamical states in both synthetic and real-world time series data.

I. INTRODUCTION

Understanding and classifying emergent dynamical states in real-world and engineered systems remains a fundamental challenge due to the intrinsic complexity of their physical mechanisms and the involvement of multiple interacting parameters. However, the increasing availability of large scale time series data and advances in high performance computing open new opportunities to uncover meaningful dynamical patterns by integrating data driven approaches with computational modeling. Many real systems such as biological, climate, and social systems and engineered systems including mechanical, electronics and power grid systems often generate nonlinear time series that encode a variety of rich dynamical behaviors, including periodic, quasiperiodic, chaotic, and hyperchaotic regimes [1–5]. Accurate identification of these behaviors is essential not only for advancing our understanding of the underlying physics but also for anticipating critical transitions, detecting early warning signals, and designing robust prediction and control strategies [6–9].

Traditionally, the classification of time series from dynamical systems relies on techniques such as Lyapunov exponent spectra [10, 11]. However, this approach becomes impractical in the presence of stochasticity or when the governing equations do not fully capture the underlying dynamics of the system. Moreover, estimating Lyapunov exponents from empirical data requires large volumes of clean stationary signals, which limits their applicability in real-world scenarios [12]. Thus, developing methods to capture the inherent dynamics of a system from empirical time series data remains a challenging and

active area of research.

Recurrence quantification analysis (RQA) has emerged as one of the most powerful techniques for uncovering dynamical states from time series data, whether derived from dynamical models or empirical measurements. RQA has been successfully applied across a wide range of disciplines, for example, in biological systems for the analysis of heart rate variability analysis [13] and neural activity characterization [14]; in climate science to identify climate change dynamics [15–17]; and in engineering systems for the prediction of mechanical failures [18]. This method analyzes recurrence patterns in the reconstructed phase space from data using recurrence plots (RPs). Introduced by Eckmann et al. [19], RPs provide a visual representation of the times when the state of the system returns close to the states visited previously [20]. They reveal complex dynamical features, such as periodicity, laminar phases, drifts, and chaotic bursts, that often escape detection by traditional linear or spectral methods [21, 22]. RQA extends the basic recurrence plot framework by introducing a set of quantitative measures, such as recurrence rate, determinism, laminarity, and entropy, that enable systematic analysis of the underlying dynamics [23]. However, as demonstrated in a recent study [24], these measures often exhibit overlapping value ranges across different dynamical regimes, making it difficult to uniquely identify a specific state based on any single measure. Reliable classification, therefore, typically requires a carefully chosen combination of multiple RQA features, underscoring the limitations of relying on individual measures for accurate identification of dynamical states.

With recent progress in machine learning, a new re-

search direction has emerged that integrates the recurrence based measures with machine learning algorithms for automated classification of dynamical regimes. Several studies have used RQA derived features as input to standard machine learning or deep learning models that demonstrated improved classification performance [24, 25]. However, the computational cost of extracting RQA features, especially for long or high dimensional time series, remains a significant limitation [26]. To mitigate this, faster alternatives have been proposed, such as parametric RQA [14] and symbolic recurrence quantification [27].

A promising alternative bypasses the need for explicit feature extraction altogether by feeding recurrence plots directly into deep learning models, particularly convolutional neural networks (CNNs). CNNs, widely used in image classification, automatically learn hierarchical spatial features through convolutional layers. This image based strategy enables CNNs to extract discriminative patterns directly from recurrence plots without requiring prior feature engineering. Notable applications include arrhythmia detection from ECG data [25], activity recognition using wearable sensors [28], control system development [29], and parameter estimation in nonlinear systems [30]. These studies show that RP based deep learning models can match or even outperform traditional feature based approaches, offering greater scalability and adaptability. Despite these advances, CNN architectures suffer from vanishing gradients, which hinder the training of deeper models. This challenge is largely resolved with the introduction of ResNet architectures [31], which use residual connections to preserve gradient flow and enable deep network training.

In our study, we propose a deep learning model that incorporates ResNet-50[31] as a backbone for feature extraction from recurrence plots, followed by two parallel branches inspired by the DSRNet architecture [32]. These branches are designed to emphasize features corresponding to various directional edges, which are important for recurrence plots. We then compare the performance of our proposed model against a standard ResNet-50 implementation. In the proposed deep learning model, we provide RPs as input images, and train the model to classify time series into one of the six categories: periodic, quasi-periodic, chaotic, hyperchaotic, white noise, or red noise. We demonstrate that our approach offers higher accuracy and greater computational efficiency compared to traditional RQA-based methods and other CNN-based methods that uses RPs as input images.

Our paper is organized as follows. In section II we discuss the methodology for the classification of nonlinear time series by integrating machine learning models and recurrence plots. Section III presents the results that show the performance of our proposed model for simulation and real-world data sets. In the concluding section IV, we summarize the results and indicate promising future extensions for our model.

II. METHODOLOGY

To construct the training dataset, we first simulate a set of standard dynamical systems along with noisy data sets, as summarized in Table I. From the resulting time series, we reconstruct the phase space using Takens' embedding theorem. Recurrence plots are then generated from these reconstructed trajectories to capture the intrinsic recurrence structure of the underlying dynamics.

These RPs are used as input features for the proposed deep learning framework, which is designed to classify distinct dynamical regimes and noise types. A schematic representation of the overall methodology that includes a systematic way of classification of time series using deep learning model is shown in Figure 1. Comprehensive details on time series generation, RP construction, and the architecture of the proposed deep learning model are provided in the following subsections.

A. Time series datasets

To generate the time series datasets, we simulate standard nonlinear dynamical systems as listed in Table I using the RK45 integrator. By systematically varying the model parameters and initial conditions, we ensure a broad coverage of nonlinear behaviors. For instance, Chen 4D and Lorenz 4D systems are used to generate time series exhibiting chaotic, hyperchaotic, and periodic dynamics. We use the third system to generate time series that show quasi-periodic behavior. For each simulated system, we use a single time series corresponding to the x variable (see Fig. 1(a)). In addition, we generate noisy signals, of Gaussian white noise and red noise, using the algorithm described by Timmer and Koenig[33]. We also produce additional noisy datasets by adding Gaussian noise to the state variables of the deterministic systems. The standard deviation of the noise is set as a fixed proportion of the original data, as described below:

$$x_{\text{noisy}}(t) = x(t) + \mathcal{N}(0, \sigma_n^2), \quad (1)$$

with $\sigma_n = \alpha \cdot \sigma_x$, $\alpha \sim \mathcal{U}(0, 0.05)$,

where σ_x denotes the standard deviation of the data $x(t)$ obtained from the dynamical system, and σ_n denotes the standard deviation of noise. We normalize each dataset before using it to reconstruct the phase space and analyze recurrence features, as detailed in the following section.

B. Reconstruction of Phase space

From the normalized univariate time series, we reconstruct the system's phase space using Takens' embedding theorem [37]. According to this theorem, the topological structure of the original multi dimensional state space

TABLE I. Dynamical and stochastic systems used to generate different classes of time series.

System	Equations / Algorithms	Parameters	Class
Chen 4D[34]	$\frac{dx}{dt} = a(y - x) + e y z$ $\frac{dy}{dt} = cx - dxz + y + u$ $\frac{dz}{dt} = xy - bz$ $\frac{dw}{dt} = -k y$	$a = 35, b = 4.9, c = 25, d = 5, e = 35$ $k = 100$ $k = 315$ $k = 495$	Hyperchaotic Chaotic Periodic
Lorenz 4D[35]	$\frac{dx}{dt} = a(y - x)$ $\frac{dy}{dt} = bx - xz - cy + w$ $\frac{dz}{dt} = xy - dz$ $\frac{dw}{dt} = -k y - r w$	$a = 12, b = 23, c = 1, d = 2.1, r = 0.2$ $k = 4$ $k = 0.1$ $k = 18, 20$	Hyperchaotic Chaotic Periodic
Quasiperiodic System[36]	$\frac{dx}{dt} = y$ $\frac{dy}{dt} = (\lambda + z + x^2 - \beta x^4)y - \omega_0^2 x$ $\frac{dz}{dt} = b(\varepsilon - z) - ky^2$	$\lambda = -1, c = 4, \beta = \frac{1}{18},$ $\omega_0 = 2\pi, b = 1, k = 0.02$	Quasiperiodic
Stochastic Data[33]	$N_1, N_2 \sim \mathcal{N}(0, 1)$ $S(f_k) \sim f_k^{-\beta}$ $F(f_k) = \sqrt{\frac{S(f_k)}{2}} (N_1 + iN_2)$ $x(t) = \mathcal{F}^{-1}[F(f_k)]$	$\beta = 0$ $\beta = 2$	White Noise Red Noise

can be recovered by constructing delay vectors with appropriate delay and embedding dimension.

$$\mathbf{x}(t) = (x(t), x(t + \tau), x(t + 2\tau), \dots, x(t + (d - 1)\tau)) \quad (2)$$

where τ is the embedding delay, and d is the embedding dimension.

Various techniques are available to estimate appropriate values for the time delay τ and the embedding dimension d , which are essential to reconstruct the trajectory of the system from a single scalar time series. In our study, we employ the mutual information method [38] to estimate τ . The first local minimum of the mutual information curve is typically selected as the optimal delay, as it marks the point at which successive values of the time series become sufficiently independent for effective phase space reconstruction. Although the precise value of the delay may depend on the resolution of the time series, the method remains robust provided that the search is performed over a sufficiently large range to capture the local minimum.

To determine the embedding dimension d , we use the method of False Nearest Neighbors (FNN), following the approach proposed by Kennel et al. [39]. The underlying idea is that if the reconstructed trajectory is folded onto itself in a lower dimensional space, it results in a higher number of false neighbors. The knee point at which this number levels off to zero indicates a suitable embedding dimension that preserves the system's topology.

With the appropriate choice of τ and d , the original univariate time series is transformed into a sequence of embedded vectors. These vectors are organized into a matrix \mathbf{X} as follows:

$$\mathbf{X} = \begin{bmatrix} x_1 & x_{1+\tau} & \cdots & x_{1+(d-1)\tau} \\ x_2 & x_{2+\tau} & \cdots & x_{2+(d-1)\tau} \\ x_3 & x_{3+\tau} & \cdots & x_{3+(d-1)\tau} \\ \vdots & \vdots & \ddots & \vdots \\ x_N & x_{N+\tau} & \cdots & x_{N+(d-1)\tau} \end{bmatrix} \quad (3)$$

where each row represents a delay vector or an embedded vector, and plotting these vectors in the reconstructed phase space reveals the underlying structure of the system, capturing its essential dynamical properties. Thus, this matrix effectively reconstructs the phase space trajectory and serves as the basis for subsequent recurrence analysis.

C. Recurrence Plots

Recurrence plots provide a two dimensional representation of the times at which a dynamical system revisits states that are close to previously encountered ones, within a predefined distance threshold ϵ . Given a delay embedded matrix \mathbf{X} in Eq. 3, the recurrence matrix \mathbf{R} is defined as:

$$R_{i,j} = \Theta(\epsilon - \|\mathbf{x}_i - \mathbf{x}_j\|),$$

$$\text{where } \Theta(u) = \begin{cases} 1 & \text{if } u \geq 0 \\ 0 & \text{if } u < 0 \end{cases} \quad (4)$$

Choosing an appropriate threshold ϵ is critical for constructing meaningful recurrence plots, as it determines which state pairs are considered recurrent and thereby influences the actual dynamical state of the system. An

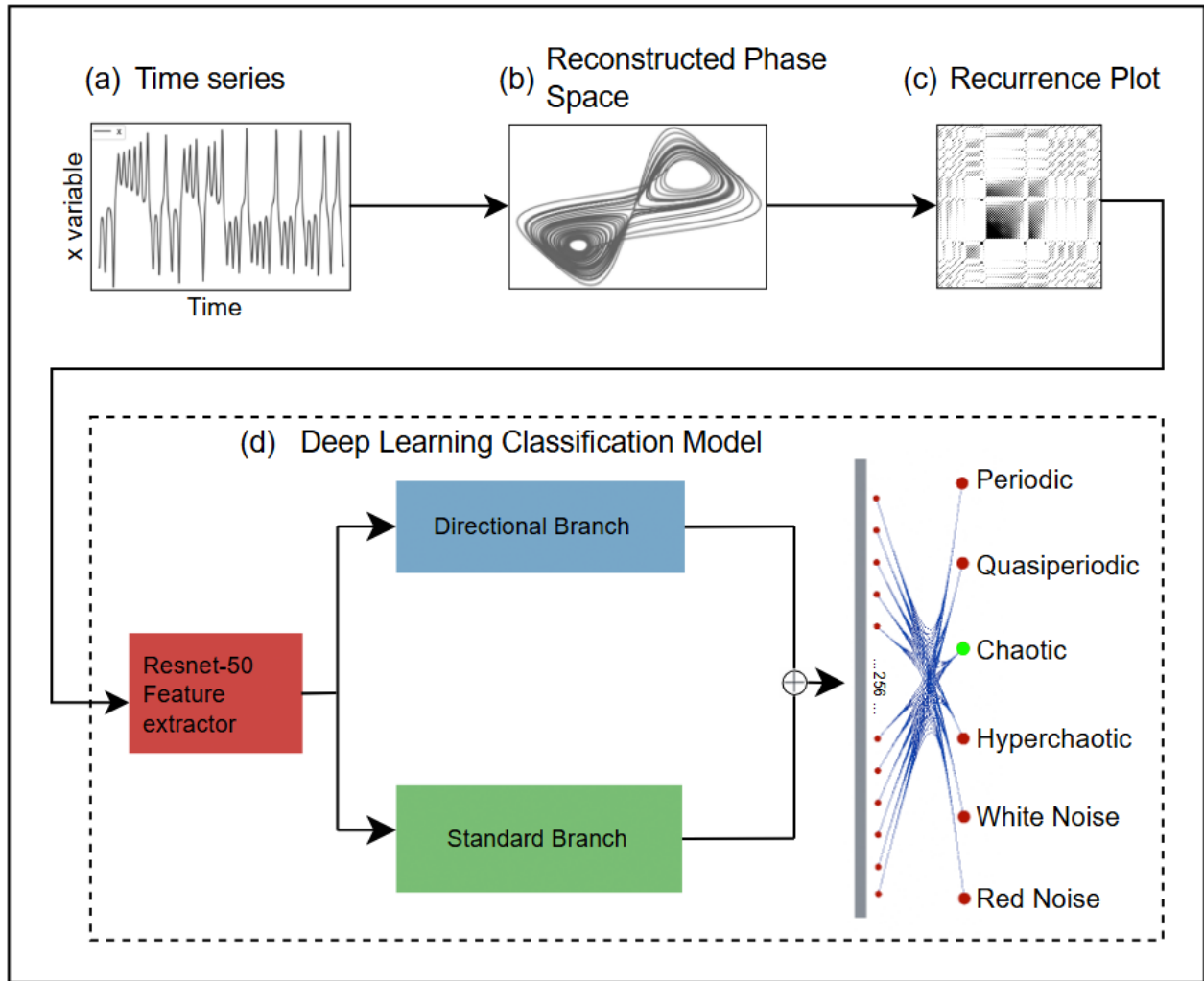


FIG. 1. **Classification of time series.** Schematic representation of the proposed methodology for classifying time series using RPs as input to a deep learning model. (a) We begin by selecting a normalized time series from some simulated dynamical systems and noise generator as listed in Table I (b) The phase space of the selected time series is reconstructed using Takens' embedding theorem. (c) A recurrence plot is then generated from the embedded trajectory using a suitable recurrence threshold ϵ . (d) The resulting RP is resized and used as the input to the deep learning model. In this model, ResNet-50 helps to extract features from RP. Its output is processed through two parallel branches: one capturing spatial features and the other emphasizing directional sensitivity through fixed orientation filters. The outputs from both branches are concatenated and passed through a dense layer. Finally, a softmax layer generates class wise probabilities, from which the most probable dynamical state is identified. For example, if the input time series is chaotic, the output layer assigns a higher probability to the chaotic class.

optimal threshold preserves significant features of the dynamics while excluding noise-induced or irrelevant recurrences [40]. If ϵ is too small, the recurrence plot may contain very few recurrence points, leading to the omission of important dynamical patterns. Conversely, if ϵ is too large, the plot becomes overly dense, which can obscure important structures such as diagonal lines that reflect periodic or quasi-periodic behavior.

To select an appropriate threshold, common approaches include fixing ϵ as a percentage of the signal's standard deviation [41], or adjusting it to maintain a

fixed recurrence rate across datasets [21]. In our study, we set the threshold ϵ to achieve a fixed recurrence rate of 5%. To do this, we compute all pairwise distances and select the distance value at which 5% of the distances are smaller than or equal to it, as the threshold ϵ .

D. Deep Learning Models for Classification

We first implement a single-branch deep learning model based on the ResNet-50 architecture as a base-

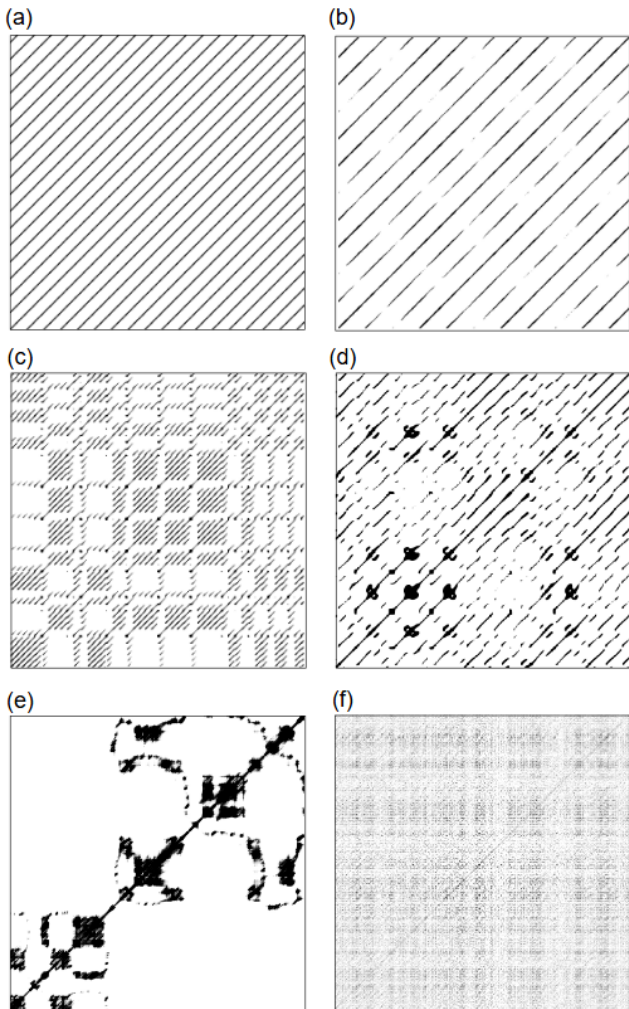


FIG. 2. **Representative recurrence plots.** These plots are obtained from the univariate time series corresponding to the following six classes: (a) Periodic (Lorenz 4D), (b) Quasiperiodic, (c) Chaotic (Lorenz 4D), (d) Hyperchaotic (Chen 4D), (e) Red Noise, and (f) White Noise.

line to compare with our proposed dual-branch model. This baseline model utilizes a pre-trained ResNet-50 network [31], trained on the ImageNet dataset[42], to extract spatial features from input RPs. We apply a Global Average Pooling (GAP) layer to the final convolutional output of the ResNet-50 backbone. The resulting pooled features are passed through a fully connected layer with 256 neurons and ReLU activation to capture nonlinear relationships. To avoid overfitting, a dropout layer is applied with a rate of 0.5. Finally, a softmax output layer produces a probability distribution over the target classes.

Building upon this, we implement a dual-branch deep learning model inspired by the DSRNet architecture [32]. As in the baseline, a pre trained ResNet-50 backbone (trained on ImageNet) is used to extract feature maps from the input RPs. These feature maps are then pro-

cessed through two parallel branches. The standard branch mirrors the baseline model, applying a GAP layer to the final convolutional output of the ResNet-50 backbone. The directional branch begins by reducing the depth of the ResNet feature maps to a single channel using a 1×1 convolution. Following the design of DSRNet, eight fixed 3×3 directional convolution kernels are applied to highlight edge information along eight principal orientations: horizontal (0°), vertical (90°), and diagonals (45° , 135° , 180° , 225° , 270° , 315°). These directionally filtered maps are further processed by a learnable 3×3 convolution layer, followed by GAP.

The outputs of the standard and directional branches are concatenated and passed through a fully connected layer with 256 neurons and ReLU activation. A Dropout layer (rate = 0.5) is again applied for regularization, and the final softmax layer maps the combined representation to the class probabilities.

III. RESULTS

The goal of this work is to accurately identify and classify distinct dynamical behaviors and noisy patterns using our developed machine learning model trained on RPs. We generate a total of 1800 RPs per class from various dynamical systems and noises, as shown in Table I. Each deterministic class includes 800 RPs from the respective system and 800 noise-augmented variants derived from the same system, as described in Section II A. The complete dataset contains six distinct classes. Representative examples of RPs from each class are presented in Figure 2. The dataset is partitioned into training and testing sets using an 80:20 split, ensuring that the testing data remains completely unseen during the training process. All images are resized to 800×800 pixels and converted to `float16` precision to optimize memory usage. Model training is performed using the Adam optimizer with a low learning rate 10^{-7} to ensure stable convergence. To prevent overfitting, early stopping is applied with a patience parameter of 2, monitored on the test error. The model is trained for a maximum of 100 epochs with a batch size of 8.

To enhance prediction accuracy, we apply a test-time augmentation strategy in which each input image is rotated in multiple orientations and cropped by up to 10%, while preserving the original aspect ratio. Predictions are generated for all augmented variants of the same image, and the class with the highest average confidence across these predictions is selected as the final output. This ensemble-like approach improves robustness to minor variations in recurrence plot appearance and mitigates overfitting to specific orientations or features.

To assess the performance of the classification scheme, we compute per-class accuracy in addition to confusion matrices and standard classification metrics, as follows: Given a confusion matrix $\mathbf{C} \in \mathbb{N}^{K \times K}$, where $C_{i,j}$ denotes the number of samples whose true class is i and predicted

class is j , and K denotes the number of classes, the accuracy per class for class i is defined as:

$$\text{Accuracy}_i = \frac{C_{i,i}}{\sum_{j=1}^K C_{i,j}}, \quad \text{for } i = 1, 2, \dots, K \quad (5)$$

where, $C_{i,i}$ is the number of correctly predicted samples for the class i , $\sum_{j=1}^K C_{i,j}$ is the total number of samples belonging to the class i . This metric reflects how well the model performs individually for each class.

A. Classification of simulated time series data

To evaluate the performance of both trained machine learning models, ResNet-50 and our proposed dual-branch model, we first validate them on simulated time series data drawn from the same distribution as the training set, generated using the systems listed in Table I. Both models demonstrate comparable performance on this simulated dataset and therefore, we present only the results obtained from our dual-branch model.

The confusion matrix in Figure 3 provides a representative overview of classification performance across all six classes. The diagonal elements indicate correct classifications, while off-diagonal elements represent misclassifications. Figure 3 shows that all predictions lie on the diagonal, indicating perfect classification of the test dataset. The evaluation metrics of the model, including precision, recall, F1 score, and per-class accuracy, all indicate 100% performance, further confirming that the model achieves an overall accuracy of 100%.

Given the perfect accuracy, we check the possibility of model's overfitting. Overfitting typically occurs when a model memorizes the training data and fails to generalize, often indicated by a divergence between train and test accuracies during training. However, as shown in Figure 4, both train and test accuracies remain consistently high and closely aligned throughout the training process, suggesting that overfitting is unlikely in our case. This robustness may be attributed to the similarity between the train and test datasets, as well as the use of early stopping, which terminates training before the onset of overfitting.

To further validate the model using simulated datasets, we evaluate its performance on data generated from the Lorenz 3D[43] and Rössler 3D[44] systems, which are not included during the training phase. For the Lorenz 3D system, we generate time series from both chaotic and periodic regimes and construct the corresponding recurrence plots. These plots are accurately classified as chaotic and periodic, respectively, by both the ResNet-50 model and the proposed dual-branch model. Similarly, for the Rössler 3D system, we generate recurrence plots from chaotic and periodic regimes, which are also correctly identified by both models.

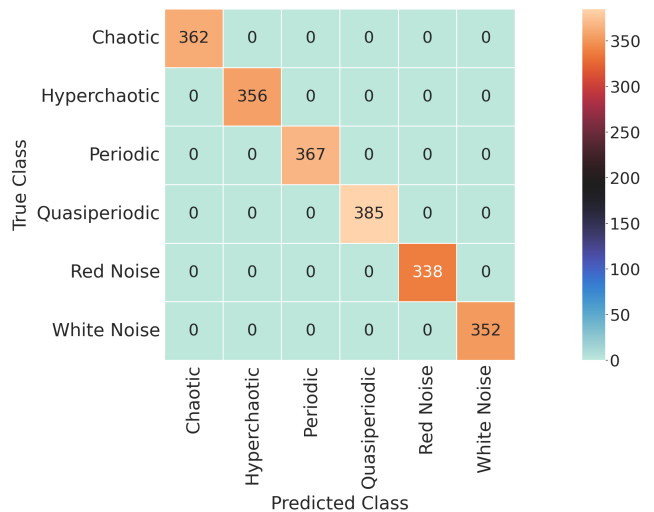


FIG. 3. **Confusion matrix.** The matrix illustrates the classification performance of the dual-branch model on simulated test datasets. The diagonal cells show how many recurrence plots are correctly classified, while the off-diagonal cells show how many are misclassified into other classes.

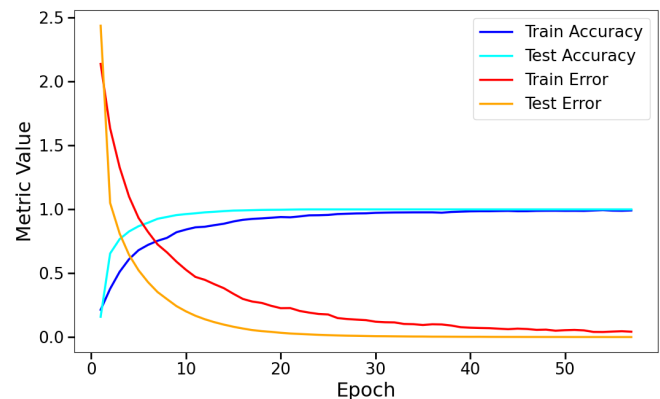


FIG. 4. **Comparison of accuracy and error rates between the training and testing phases for the dual-branch model.** Our dual-branch model exhibits similar trends and convergence in accuracy and error for both training and testing time series data, indicating that the model does not overfit.

B. Classification of empirical time series

To further evaluate the generalizability of our trained deep learning model, we test it on experimental time series data. As a first example, we use the time series data obtained from the Chua circuit. We generate and pass the recurrence plots of different time series lengths to the models in order to test their performance on varying pattern scales within the recurrence plots. The cropping and the corresponding recurrence plots are shown in Figure 5. Both ResNet-50 and the proposed dual-branch model correctly classify the Chua circuit signal as chaotic, consistent with the well-established chaotic dynamics of

the Chua system [5, 45].

We further validate the model using the light curve data from three variable stars, AC Her, SX Her, and Chi Cygni, sourced from the AAVSO database (<https://www.aavso.org/data-download>). Figure 6 presents the light curves and their corresponding recurrence plots. The light curves for AC Her and SX Her span 14 years, beginning on 20 September 1980, while the Chi Cygni light curve covers a 5-year period starting on 20 September 2019. To ensure consistent sampling and reduce observational noise, we smooth the AC Her and SX Her light curves using a 5-day rolling average, and the Chi Cygni light curve using a 20-day rolling average. All light curves are then interpolated using cubic splines with a smoothing parameter of $s = 0.065$.

The light curve of Chi Cygni is correctly classified as periodic by both the ResNet-50 and dual-branch models, in agreement with previous studies [46]. However, the ResNet-50 model misclassifies AC Her as white noise and SX Her as hyperchaotic, contradicting earlier findings that identify both stars as exhibiting chaotic dynamics [47, 48]. In contrast, our proposed dual-branch model correctly classifies both AC Her and SX Her as chaotic, in alignment with prior literature. Hence, we conclude that the proposed dual-branch model provides a more reliable framework than the ResNet-50 model for accurately identifying the underlying dynamics of empirical time series.

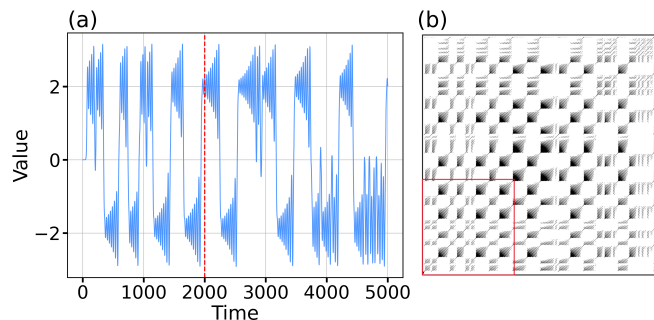


FIG. 5. **Experimental data from Chua’s circuit.** (a) Time series obtained experimentally from Chua’s circuit. The red line indicates the cropped portion of the timeseries (b) Corresponding RP and the red box highlights the region in the RP corresponding to only the cropped portion shown in (a).

IV. CONCLUSION

In this work, we introduce a new deep learning model that accurately predicts the inherent dynamical nature of both synthetic and empirical time series data. The central question we address is one of broad relevance: *Can we reliably infer the underlying dynamics of real-world time series data?* To answer this, we integrate recurrence plots, extracted via phase-space reconstruction us-

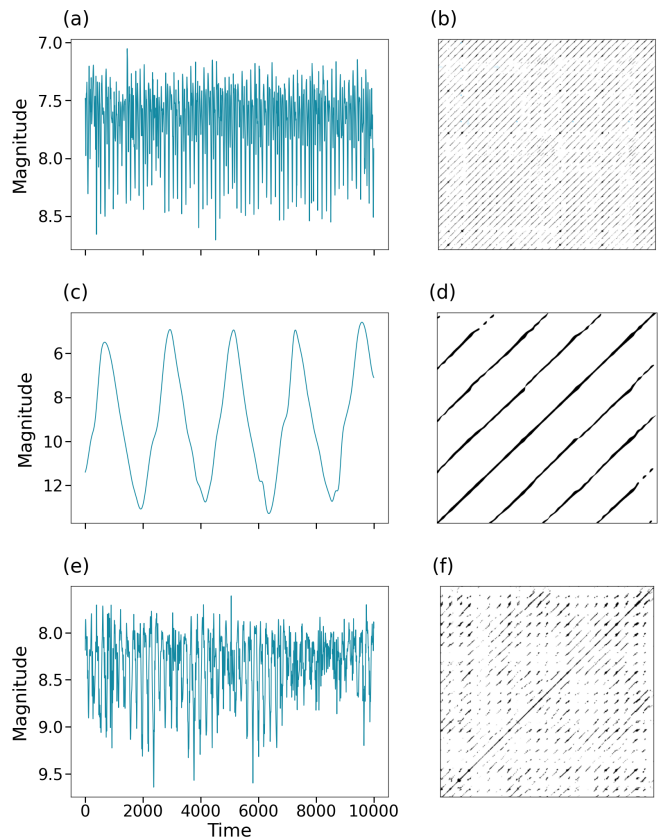


FIG. 6. **Light curves and corresponding recurrence plots for variable stars.** The left column (a, c, e) shows the light curves, while the right column (b, d, f) presents the corresponding recurrence plots for the stars AC Her, Chi Cygni, and SX Her, respectively.

ing Takens’ embedding theorem, with deep learning models that learn to identify complex dynamical structures directly from the RPs. This approach demonstrates high accuracy and strong generalizability, making it a scalable and robust solution for dynamical states classification.

We implement a customized dual-branch deep learning model that takes RP images as inputs. These RPs are generated from nonlinear time series obtained through simulations of various dynamical systems and noise data. Our model can classify these time series into six distinct classes: periodic, quasi-periodic, chaotic, hyperchaotic, white noise, and red noise. The architecture of our model builds on a ResNet-50 backbone and incorporates two parallel branches: one that captures global spatial features and another that extracts directional and edge-based patterns, enhancing the model’s classification performance over the standard ResNet-50.

In summary, our framework demonstrates robust classification performance across synthetic, experimental, and observational datasets. Notably, the trained dual-branch model accurately classifies unseen simulated time series from the Lorenz 3D and Rössler 3D systems, as well as experimental data from a Chua’s circuit and as-

TABLE II. Comparison of the performance of ResNet-50 and the new dual-branch model in the classification of unseen simulated and experimental time series data

Time Series	ResNet-50	Dual-Branch Model	True Class
Simulated Time Series Data			
Lorenz 3D	Chaotic	Chaotic	Chaotic [43]
	Periodic	Periodic	Periodic [43]
Rossler 3D	Chaotic	Chaotic	Chaotic [44]
	Periodic	Periodic	Periodic [44]
Experimental/Observational Time Series Data			
Chua Circuit	Chaotic	Chaotic	Chaotic [5]
Chi Cygni	Periodic	Periodic	Periodic [46]
AC Her	White Noise	Chaotic	Chaotic [48]
SX Her	Hyperchaotic	Chaotic	Chaotic [47]

tronomical light curves from variable stars AC Her, SX Her, and Chi Cygni, as shown in Table II. This demonstrates the model’s applicability to real-world data and reinforces the potential of using recurrence based deep learning models for determining the inherent dynamics of the system. We observe that our dual-branch model outperforms than other convolutional neural networks models that have been used to classify the dynamical behavior using RPs as inputs.

We also compared with traditional approaches that rely on recurrence quantification measures and recurrence network metrics [24], our method offers a significantly more efficient alternative. It eliminates the need for manual feature engineering by learning discriminative features directly from RP images. Our results show that high classification accuracy can be achieved without computing various recurrence measures.

Looking ahead, several directions could further extend the capabilities of our model. A promising approach involves detecting dynamical transitions within time series by segmenting recurrence plots along the line of identity (LOI) using our model on transition-rich data to identify these substructures, similar to time-dependent RQA techniques [40]. Another enhancement includes combining our approach with model-based generative frameworks, such as delay embedding and deep delay autoencoders [49], to synthesize training data from partial observations of unknown systems. This could reduce dependence on fully simulated datasets and improve performance under limited data conditions.

In conclusion, this work establishes a new deep learning model that takes recurrence plots as images and

offers a powerful, efficient, and generalizable framework for classifying dynamical states. It opens new possibilities for analyzing complex time series in diverse fields such as physics, neuroscience, astrophysics, and beyond.

V. ACKNOWLEDGMENTS

We acknowledge with thanks the variable star observations from the AAVSO International Database contributed by observers worldwide and used in this research. We also thank Prof. K. Murali for providing Chua circuit used in validating our model. AM and CM acknowledge financial support from ANRF, India (Grant No. EEQ/2023/001080), and DST, India (INSPIRE Grant No. IFA19-PH248). AM is also thankful to Corina Simon for facilitating access to the NVIDIA A100 GPU via Google Colab.

VI. DATA AVAILABILITY

The time series datasets of standard systems used in this study are generated by simulating the dynamical models listed in Tables II and II using the RK45 integrator. The experimental time series data for the Chua circuit are provided by Prof. K. Murali’s lab at Anna University, India. Time series of variable stars (light curves) are obtained from the AAVSO database (<https://www.aavso.org/data-download>).

[1] H. Kantz and T. Schreiber, *Nonlinear Time Series Analysis* (Cambridge University Press, Cambridge, 2003).
[2] C. Meena, S. Kumari, A. Sharma, and S. Sinha, *Chaos, Solitons & Fractals* **104**, 668 (2017).
[3] J. P. Crutchfield, J. D. Farmer, N. H. Packard, and R. S. Shaw, *Scientific American* **255**, 46 (1986).
[4] C. Meena, P. D. Rungta, and S. Sinha, *The European Physical Journal B* **93**, 1 (2020).

[5] M. Lakshmanan and K. Murali, *Chaos in nonlinear oscillators: controlling and synchronization*, Vol. 13 (World scientific, 1996).
[6] M. Scheffer, J. Bascompte, W. A. Brock, V. Brovkin, S. R. Carpenter, V. Dakos, H. Held, E. H. Van Nes, M. Rietkerk, and G. Sugihara, *Nature* **461**, 53 (2009).
[7] T. M. Lenton, *Nature Climate Change* **1**, 201 (2011).

- [8] C. Meena, P. D. Rungta, and S. Sinha, *Plos one* **12**, e0183251 (2017).
- [9] E. Schöll and H. G. Schuster, eds., *Handbook of Chaos Control*, 2nd ed. (Wiley-VCH, 2008).
- [10] A. Bespalov and N. Polyakhov, *World Appl. Sci* **26**, 157 (2013).
- [11] A. Wolf, J. B. Swift, H. L. Swinney, and J. A. Vastano, *Physica D: nonlinear phenomena* **16**, 285 (1985).
- [12] Y. Zou, R. V. Donner, J. F. Donges, N. Marwan, and J. Kurths, *Chaos: An Interdisciplinary Journal of Nonlinear Science* **20**, 043130 (2010).
- [13] N. Marwan, N. Wessel, U. Meyerfeldt, A. Schirdewan, and J. Kurths, *Phys. Rev. E* **66**, 026702 (2002).
- [14] S. Ramdani, A. Boyer, S. Caron, F. Bonnetblanc, F. Bouchara, H. Duffau, and A. Lesne, *Pattern Recognition* **109**, 107572 (2021).
- [15] Z. Zhao, S. Li, J. Gao, and Y. Wang, *International Journal of Bifurcation and Chaos* **21**, 1127 (2011).
- [16] M. H. Trauth, A. Asrat, W. Duesing, V. Foerster, K. H. Kraemer, N. Marwan, M. A. Maslin, and F. Schaebitz, *Climate Dynamics* **53**, 2557 (2019).
- [17] J. John Bejoy and G. Ambika, *Chaos: An Interdisciplinary Journal of Nonlinear Science* **34**, 043150 (2024).
- [18] Y. Qian, R. Yan, and M. Shan, in *Proceedings of the IEEE 2012 Prognostics and System Health Management Conference (PHM-2012 Beijing)* (IEEE, 2012) pp. 1–5.
- [19] J.-P. Eckmann, S. O. Kamphorst, and D. Ruelle, in *Turbulence, Strange Attractors and Chaos* (World Scientific, 1995) pp. 441–445.
- [20] G. Ambika and K. P. Harikrishnan, *Methods of nonlinear time series analysis and applications: A review*, in *Dynamics and Control of Energy Systems*, edited by A. Mukhopadhyay, S. Sen, D. N. Basu, and S. Mondal (Springer Singapore, Singapore, 2020) pp. 9–27.
- [21] N. Marwan, M. Carmen Romano, M. Thiel, and J. Kurths, *Physics Reports* **438**, 237 (2007).
- [22] D. Kugiumtzis, O. Lingjærde, and N. Christophersen, *Physica D: Nonlinear Phenomena* **112**, 344 (1998).
- [23] C. L. W. Jr. and N. Marwan, eds., *Recurrence Quantification Analysis*, 1st ed., *Understanding Complex Systems* (Springer Cham, 2015) pp. XIV+421.
- [24] D. Thakur, A. Mohan, G. Ambika, and C. Meena, *Chaos: An Interdisciplinary Journal of Nonlinear Science* **34** (2024).
- [25] B. M. Mathunjwa, Y.-T. Lin, C.-H. Lin, M. F. Abbod, and J.-S. Shieh, *Biomedical Signal Processing and Control* **64**, 102262 (2021).
- [26] T. Rawald, M. Sips, N. Marwan, and D. Dransch, in *Translational Recurrences: From Mathematical Theory to Real-World Applications* (Springer, 2014) pp. 17–29.
- [27] M. Caballero-Pintado, M. Matilla-García, and M. Ruiz Marín, *Chaos: An Interdisciplinary Journal of Nonlinear Science* **28** (2018).
- [28] E. Garcia-Ceja, M. Z. Uddin, and J. Torresen, *Procedia computer science* **130**, 157 (2018).
- [29] A. L. Fradkov and A. Y. Pogromsky, *Introduction to control of oscillations and chaos* (World Scientific, 1998).
- [30] L. Lober, M. Palmero, and F. Rodrigues, *arXiv preprint arXiv:2410.23408* (2024).
- [31] K. He, X. Zhang, S. Ren, and J. Sun, in *2016 IEEE Conference on Computer Vision and Pattern Recognition (CVPR)* (2016) pp. 770–778.
- [32] W. Zhai, Y. Cao, Z.-J. Zha, H. Xie, and F. Wu, in *Proceedings of the IEEE/CVF Conference on Computer Vision and Pattern Recognition* (2020) pp. 11010–11019.
- [33] J. Timmer and M. Koenig, *Astronomy and Astrophysics*, v. 300, p. 707 **300**, 707 (1995).
- [34] Z. Chen, Y. Yang, G. Qi, and Z. Yuan, *Physics Letters A* **360**, 696 (2007).
- [35] Y. Li, X. Liu, G. Chen, and X. Liao, *International Journal of Circuit Theory and Applications* **39**, 865 (2011).
- [36] A. Kuznetsov, Y. Sedova, and N. Stankevich, *Chaos Solitons & Fractals* **169**, 113278 (2023).
- [37] L. Noakes, *International Journal of Bifurcation and Chaos* **1**, 867 (1991).
- [38] E. Tan, S. Algar, D. Corrêa, M. Small, T. Stemler, and D. Walker, *Chaos: An Interdisciplinary Journal of Nonlinear Science* **33**, 032101 (2023).
- [39] M. B. Kennel, R. Brown, and H. D. I. Abarbanel, *Phys. Rev. A* **45**, 3403 (1992).
- [40] N. Marwan, *International Journal of Bifurcation and Chaos* **21**, 1003 (2011).
- [41] B. Ambrozkiewicz, N. Meier, Y. Guo, G. Litak, and A. Georgiadis, *IOP Conference Series: Materials Science and Engineering* **710**, 012014 (2019).
- [42] O. Russakovsky, J. Deng, H. Su, J. Krause, S. Satheesh, S. Ma, Z. Huang, A. Karpathy, A. Khosla, M. Bernstein, *et al.*, *International journal of computer vision* **115**, 211 (2015).
- [43] É. Ghys, *The lorenz attractor, a paradigm for chaos*, in *Chaos: Poincaré Seminar 2010*, edited by B. Duplantier, S. Nonnenmacher, and V. Rivasseau (Springer, Basel, 2013) pp. 1–54.
- [44] K. M. Ibrahim, R. K. Jamal, and F. H. Ali, in *Journal of Physics Conference Series*, *Journal of Physics Conference Series*, Vol. 1003 (IOP, 2018) p. 012099.
- [45] N. Kuznetsov, T. Mokaev, V. Ponomarenko, E. Seleznev, N. Stankevich, and L. Chua, *Nonlinear Dynamics* **111**, 5859 (2023).
- [46] C. Sterken, E. Broens, and C. Koen, *Astronomy and Astrophysics*, v. 342, p. 167-172 (1999) **342**, 167 (1999).
- [47] J. R. Buchler, Z. Kolláth, and R. R. Cadmus Jr, *The Astrophysical Journal* **613**, 532 (2004).
- [48] Z. Kolláth, J. Buchler, T. Serre, and J. Mattei, *Astronomy and Astrophysics*, v. 329, p. 147-154 (1998) **329**, 147 (1998).
- [49] J. Bakarji, K. Champion, J. Nathan Kutz, and S. L. Brunton, *Proceedings of the Royal Society A* **479**, 20230422 (2023).